*metals*

MDPI

*Article*

# The Microstructure and Mechanical Properties of 5083, 6005A and 7N01 Aluminum Alloy Gas Metal Arc-Welded Joints for High-Speed Train: A Comparative Study

**Laijun Wu [1,2], Biao Yang [1,2], Xiaohui Han [3], Guolong Ma [3], Bingxiao Xu [2], Yuhang Liu [2], Xiaoguo Song [1,2] and Caiwang Tan [1,2,*]**

[1] State Key Laboratory of Advanced Welding and Joining, Harbin Institute of Technology, Harbin 150001, China; wulaijun0721@163.com (L.W.); 21B909114@stu.hit.edu.cn (B.Y.); songxg@hitwh.edu.cn (X.S.)
[2] Shandong Provincial Key Laboratory of Special Welding Technology, Harbin Institute of Technology at Weihai, Weihai 264209, China; xubingxiao2020@163.com (B.X.); 18748783099@163.com (Y.L.)
[3] Technical Engineering Department, CRRC Qingdao Sifang Co., Ltd., Qingdao 266111, China; 13793237339@139.com (X.H.); guolongma@163.com (G.M.)
* Correspondence: tancaiwang@hitwh.edu.cn

**Abstract:** This study aimed to conduct a comparative study on the microstructure and mechanical performance of 5083, 6005A and 7N01 Al joints used in China Railway High-speed (CRH) trains. We connected 10 mm-thick plates by three-layer and three-pass gas metal arc welding (GMAW). The results indicated that 6005A and 7N01 Al joints were more sensitive to grain boundary liquation in the partially melted zone (PMZ) than 5083 Al joins. Besides, recrystallization was obtained in heat-affected zones (HAZ). The 5083 Al joints experienced the most severe recrystallization and the grain size changed from 6.32 (BM) to 32.44 (HAZ) μm duo to intracrystalline strain induced by cold-rolled processes. The 7N01 Al alloys experienced the lowest extent of recrystallization and the grain size increased from 5.32 (BM) to 22.31 (HAZ) μm. Furthermore, significant precipitate evolution in the HAZ was observed. Original thin β″ precipitates dissolved in HAZ of 6005A Al joints and transformed to the softer β phase. However, less precipitation transition was examined in 5083 and 7N01 Al joints. The precipitates' evolution produced a softening region in HAZ of 6005A joints where the hardness was only 55 HV. The microhardness profile of the other two Al joints was less affected. The tensile strength of 5083, 6005A, and 7N01 Al alloy joints reached 323, 206 and 361 MPa, respectively. The 5083 Al and 6005A Al joints failed at HAZ near the fusion line while 7N01 Al joints failed at the fusion zone owing to the high strength of the base metal. The liquation, coarse grains by recrystallization, and precipitate evolution all decreased local strength, resulting in the fracture at HAZ.

**Keywords:** aluminum alloy; GMAW joints; liquation; recrystallization; precipitates; mechanical property



**Citation:** Wu, L.; Yang, B.; Han, X.; Ma, G.; Xu, B.; Liu, Y.; Song, X.; Tan, C. The Microstructure and Mechanical Properties of 5083, 6005A and 7N01 Aluminum Alloy Gas Metal Arc-Welded Joints for High-Speed Train: A Comparative Study. *Metals* **2022**, *12*, 213. https://doi.org/10.3390/met12020213

Academic Editors: João Pedro Oliveira and Zhi Zeng

Received: 18 December 2021
Accepted: 18 January 2022
Published: 24 January 2022



## 1. Introduction

Aluminum alloys have been widely used as significant lightweight materials in aerospace, automotive and transportation industries due to their low density, high specific strength and excellent corrosion resistance [1–3]. Recently, 5083, 6005A and 7N01 aluminum alloys were adopted in China Railway High-speed (CRH) trains to meet the increasing lightweight demand and further reduce the carbon consumption. The gas metal arc welding (GMAW) is utilized to join those aluminum alloys due to the advantages of low costs and high efficiency. Although successful joining of 10 mm-thick sheets can be obtained by multi-layer and multi-pass GMAW, the multiple thermal-mechanical processing steps usually result in a coarse grain structure and softening zone in weld joints. These defects will deteriorate mechanical properties of welds in aluminum alloy applications.

The 5083 Al alloy is one of non-heat-treatable aluminum alloys possessing high work-hardening strength rate and good weldability [4]. The main alloying element in 5083Al alloy is 5 wt.% magnesium inducing strong solution-strengthening effects. Its application is mainly confirmed in a corrosive environment owing to relatively high strength and corrosion resistance [3]. The main problem of 5083Al alloy welds is grain coursing in fusion welding [5]. Liu et al. [6] pointed out that considerable softening was examined in 5083 Al alloy welds due to the formation of larger grains. Ma et al. [7] demonstrated that the grain size in the fusion zone reached 200 μm while that in the base metal was less than 50 μm, leading to a 15% decrease in tensile strength. Corigliano et al. [8] further pointed out that 5 mm 5083Al joints by single pass GMAW might fail at the heat-affected zone owing to strain concentration. The fracture behaviors of 10 mm-thick plates are not clear.

The 6005A Al alloy belongs to the Al–Mg–Si alloys and generally is preferred in manufacturing over Al-Cu-based (2xxx) and Al-Zn-based (7xxx) alloys because of lower prices [9]. It is an age-hardening aluminum alloy and usually experiences solution annealing, quenching as well as ageing before its supply [10]. The 6005A Al sheets are then strengthened through precipitation strengthening effects induced by β″ ($Mg_2Si$) phase. However, welding is a non-equilibrium thermal process leading to dissolution of the β″ phase. As a result, the strengthening effects decreased and softening was generated in weld zones [11,12]. Dong et al. [13] concluded that the high cooling rates at 20 °C/s of welding process restrained re-precipitation of β″ phase, leading to a 40% decrease in microhardness in the weld seam. In addition, Liu et al. [14,15] reported that coarse grains were also responsible for softening of 6005A Al alloy cold metal transfer (CMT) welds. Except for softening, hot-cracking sometimes also weakens the performance of 6005A Al alloy joints, which is hardly observed in 5083 Al joints [16]. The intergranular eutectic phases with low melting point in partially melted zones (PMZ) of 6005A Al alloy joints possibly melted while surrounded grains remained solid [17]. Consequently, cracking occurred under shrinking stress when welds were cooled down. Wang et al. [18] verified that unexpected microstructures and defects in 4 mm 6005A Al alloy joints produced nearly 30% strength loss. In multi-pass and multi-layer GMAW, microstructure evolution is more complex under multi thermal cycles. It is necessary to further study the microstructure and mechanical properties of 10 mm-thick 6005A Al alloy welds.

As for 7N01 Al alloy, the main alloying elements are Zn and Mg. Its tensile strength is higher than 5083 and 6005A Al alloy while corrosion resistance is relatively poor. The 7N01 Al alloy is often adopted in a framework, frame pillow beam and other key components where high strength is required in high-speed trains [19]. Al–Zn–Mg-based aluminum alloy is aging-strengthened, and natural aging (NA) or artificial aging (AA) are used to produce η phase ($MgZn_2$) [20,21]. Similar to 6005A Al alloy, softening was discovered in 7N01 joints under the influence of weld thermal cycles. Moreover, hot-cracking in 7N01 Al-welded joints is also considerable [22,23]. Li et al. [24] discovered uniform recrystallization and inclusions in 15 mm-thick metal-inert gas (MIG) welding joints, which decreased the tensile strength by 20%. However, the changes of precipitates were not examined.

In summary, some disadvantages limit the usage of the above three aluminum alloys. The weldability of 5083 Al alloy is the best but its plasticity and extrusion formability are not as good as the other two aluminum alloys. The tensile properties of 6005A or 7N01 Al alloys are much better while the weldability is not as good. Both of them suffered from softening and hot-cracking. Previous studies usually concerned the microstructure and mechanical properties of thin joints under single-pass welding. Fewer studies focus on multi-layer and multi-pass GAMW. It is necessary to conduct a comparative investigation on the three welding joints under multi thermal cycles to grasp the correlation between microstructure and mechanical properties. This research will provide further guidance for materials selection in the manufacturing of a high-speed train. Firstly, three-layer and three-pass GMAW was used to obtain welding joints of the three aluminum alloys. Secondly, the microstructures of the three joints were analyzed comparatively from the perspective of grain boundary liquation, precipitates dissolution and recrystallization. Finally, the

microhardness and tensile strength of those joints were compared. This study aimed to provide experimental data and a theoretical basis for high-quality and efficient welding of aluminum alloy for high-speed trains.

## 2. Materials and Methods

The A5083-O, 6005A-T6 and 7N01-T4 aluminum alloy plates with the dimension of 350 mm × 150 mm × 10 mm were employed as the base metal. The filler material was ER5356 wire with a diameter of 1.6 mm. The chemical compositions of utilized materials are listed in Table 1. The as-received mechanical properties of the base metal were listed in Table 2.

**Table 1.** The chemical composition of 5083, 6005A, 7N01 Al alloy and ER5356 (wt.%).

| Element | Mg | Si | Fe | Cu | Mn | Cr | Zn | Al |
|---|---|---|---|---|---|---|---|---|
| 5083 | 4.58 | 0.09 | 0.19 | 0.03 | 0.67 | 0.08 | 0.03 | Bal. |
| 6005A | 0.52 | 0.68 | 0.15 | 0.03 | 0.24 | 0.13 | 0.02 | Bal. |
| 7N01 | 1.19 | 0.05 | 0.18 | 0.16 | 0.36 | 0.16 | 4.5 | Bal. |
| ER5356 | 4.9 | 0.04 | 0.12 | 0.02 | 0.14 | 0.012 | 0.02 | Bal. |

**Table 2.** As-received mechanical properties of the base metal.

| Materials | Tensile Strength (MPa) | Yield Strength (MPa) | Elongation (%) |
|---|---|---|---|
| 5083 | 346 | 173 | 26.7 |
| 6005A | 284 | 254 | 19.5 |
| 7N01 | 374 | 264 | 15.0 |

Before welding, the aluminum alloy plates were machined with a V-shaped groove of 60°. This type of groove was selected because in actual applications a train pillow beam consists of an aluminum profile and plate. A V-shape was set to form a lock bottom structure. A welding backing was used under the aluminum plates to obtain full penetration GMAW joints. The surface of workpieces was polished by a stainless steel brush and then cleaned with acetone to remove the oxide film and oil from the surface of aluminum plates.

The aluminum alloy plates were assembled and fixed horizontally with a 1 mm assembly gap. The pure argon with a flow rate of 20 L/min was used as shielding gas. A welding power (TPS 5000, Fronius Inc., Wels, Austria) equipped with an welding robot (RTE40, IGM Inc., Wiener Neudorf, Austria) was selected for three-layer and three-pass gas metal arc welding as depicted in Figure 1. The proper welding parameters for 10 mm-thick sheets were studied in pre-experiments. First, the bead-on-plate welding was conducted by the single-factor experiment of welding current (180 A, 200 A, 220 A, 240 A, 260 A), welding voltage (20 V, 21 V, 22 V, 23 V, 24 V, 25 V) and welding speed (45 cm/min, 50 cm/min, 55 cm/min, 60 cm/min, 65 cm/min) to obtain the influence rule of welding process parameters on weld penetration and width. Second, the three-layer and three-pass welding experiments were designed and carried out based on the influence of welding process parameters on the weld penetration and width. Last, welding process parameters of three-layer and three-pass welding was optimized based on the welding formation of the joints. The optimized parameters are listed in Table 3.

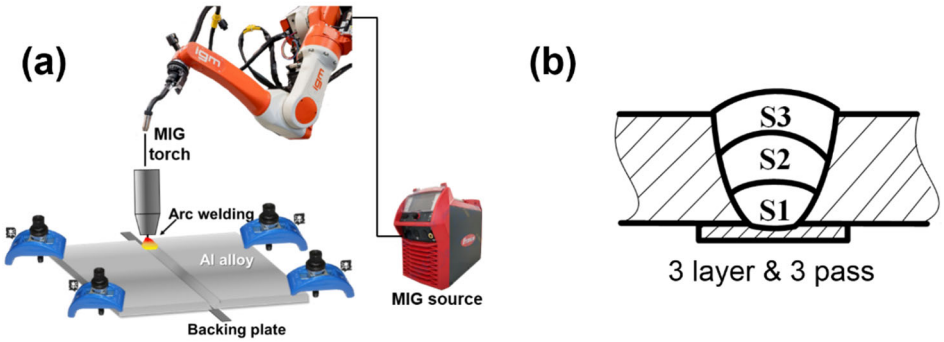


**Figure 1.** The schematic of gas metal arc welding (GMAW) of aluminum alloy. (**a**)welding diagram; (**b**) three-layer and three-pass welding layer arrangement.

**Table 3.** The process parameters employed in this study.

| Layers | Current/A | Volt/V | Velocity/cm·min$^{-1}$ | Heat Input/KJ·cm$^{-1}$ |
|---|---|---|---|---|
| Bottom layer | 256 | 23.5 | 60 | 6.0 |
| Filling layer | 256 | 23.5 | 60 | 6.0 |
| Top layer | 233 | 23.5 | 60 | 5.5 |

After welding, samples with the dimensions of 40 mm × 20 mm × 10 mm were cut perpendicular to welding direction for metallographic observation. After being sanded and polished, the cross-sections of weld joints were etched by Keller's reagent (2.5 mL $HNO_3$ + 1.5 mL HCL + 1 mL HF + 95 mL $H_2O$) for 30 s and then observed by optical microscope (Olympus DSX510, Olympus Inc., Tokyo, Japan). To observe grain structure, electron backscatter diffraction detector (EBSD) samples were prepared by electropolishing with the solution of 10% perchloric acid and 90% alcohol at 20 V for 15 s. A scanning electron microscope (SEM, Zeiss MERLIN COMPACT, Zeiss Inc., Oberkochen, Germany) equipped with a Zeiss SIGMA500 EBSD was utilized to analyze the grain structure. The evolution of precipitation phases in the joints was investigated by a transmission electron microscope (TEM, JEOL-2100, JEOL Ltd., Tokyo, Japan). In addition, specimens shaped as 3 mm × 3 mm × 1 mm cubic were cut from the base metal of three aluminum alloy, and subjected to a differential scanning calorimetry (DSC, NETZSCH STA 449F5, NETZSCH Inc., Germany), from room temperature to 700 °C at a heating rate of 10 °C/min. The microhardness of the joints was measured by a MICRO-586 microhardness tester (Buehler Inc., Lake Bluff, IL, USA) with a 100 g load and 10 s dwell time. Figure 2 shows the geometry of the tensile specimens. The tensile strength of the joints was measured by a 30 kN universal mechanical INSTRON5697 machine (INSTRON, University Ave., Norwood, MA, USA) at room temperature. The tensile tests were carried out in displacement control with crosshead speed of 2 mm/min.

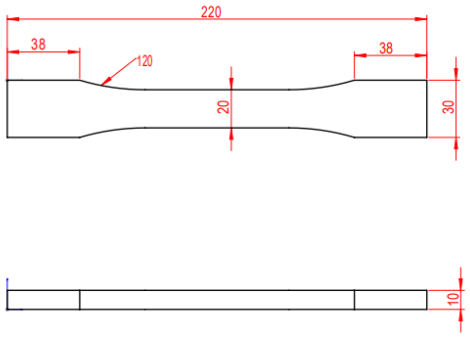


**Figure 2.** Geometry of the tensile specimens (mm).

## 3. Results and Discussion

### *3.1. Macorstructure*

The weld appearance and cross sections of 5083, 6005A and 7N01 aluminum alloy joints are given in Figure 3. It could be seen from the weld appearance that uniform and continuous weld seams with few defects were obtained. For each aluminum alloy, high-quality joints with full penetration were obtained as shown in the cross section of the joints. In addition, the weld geometry of three-layer and thee-pass joints was Y-shaped, showing a symmetrical macrostructure.

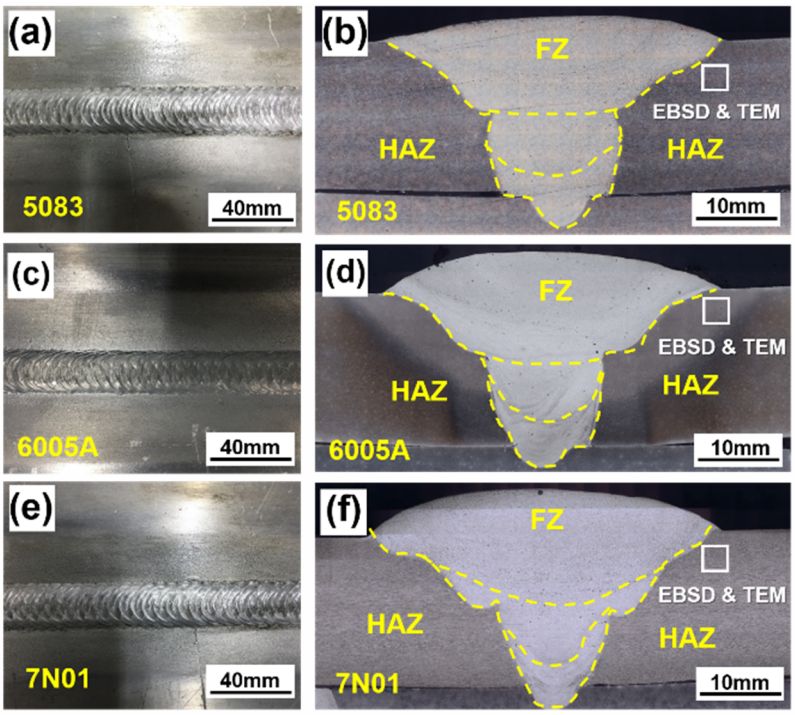


**Figure 3.** The weld appearance and cross section of welding joints: (**a**,**b**) for 5083; (**c**,**d**) for 6005A; (**e**,**f**) for 7N01.

### *3.2. Microstructure*

The cross section could be divided into a fusion zone (FZ), partial melting zone (PMZ), heat affected zone (HAZ) and the base metal (BM). The microstructure of those joints was shown in Figure 4. Similar coarse dendritic and a small amount of equiaxed crystal formed in the FZ under the welding thermal cycles as depicted in Figure 4a,d,g. The PMZ was the region immediately out the fusion zone where the peak temperature exceeded eutectic temperature [25]. In the PMZ, the individual grain melted partially, which might lead to liquation cracks. Note that the microstructure in the PMZ of the three types of aluminum alloy joints was quite different. Significant grain boundary liquation was demonstrated in the PMZ of 6005A and 7N01 Al alloy joints. Nevertheless, slight liquation of grain boundary was examined in the PMZ of 5083 Al alloy joints. The grain boundary liquation was produced by a eutectic reaction. The PMZ was adjacent to fusion line where the peak temperature was just lower than the fusion point. During the welding, a eutectic reaction ($\alpha + A_xB_y \rightarrow L$) would occur in PMZ which consisted of $\alpha$-Al matrix and $A_xB_y$ phase when the temperature of PMZ attained TE (the temperature of eutectic reaction). Generally, the $A_xB_y$ phase distributed at the grain boundary of $\alpha$-Al matrix. Therefore, eutectic remained at the grain boundary after welding. Because of different degrees of grain boundary liquation, individual grains could be clearly observed in the PMZ of 6005A and 7N01 Al alloy joints as shown in Figure 4e,h, while no obvious individual grains could be seen in that of 5083 Al alloy joints. The varied chemical composition of the base metal and grain boundary segregation were the main reason for the different degrees of grain

boundary liquation. Besides, varied microstructure was also observed in the heat-affected zone (HAZ). The HAZ could be easily identified in 6005A Al alloy joints as marked in Figure 3f because considerable recrystallization was induced by welding thermal cycles. However, in the other joints it was not as identifiable due to fewer changes in grain structure. The above results indicated that the microstructure of 5083, 6005A and 7N01 Al alloy joints in the HAZ and PMZ was quite different under the same welding thermal cycles. The most severe grain boundary liquation occurred in the PMZ of 6005A and 7N01 Al alloy while only slight grain boundary liquation was found in the PMZ of 5083 Al alloy. The boundary liquation and recrystallization significantly affected the mechanical properties, which might lead to low joint strength.

The results of EDS scanning across the FZ, PMZ, and HAZ is depicted in Figure 5. In 5083Al joints, element contents kept constant because ER5356 wire also belongs to Al-Mg series alloy as 5083Al. In 6005A joints, the Mg element decreased and the content of Si element increased in PMZ and HAZ. As for the 7N01 joints, slight decrease in content of Mg element and increase in content of Zn element was obtained. Mg induced solution strengthening effects and could form precipitates with other elements. The differences in element contents in those regions could affect local mechanical properties.

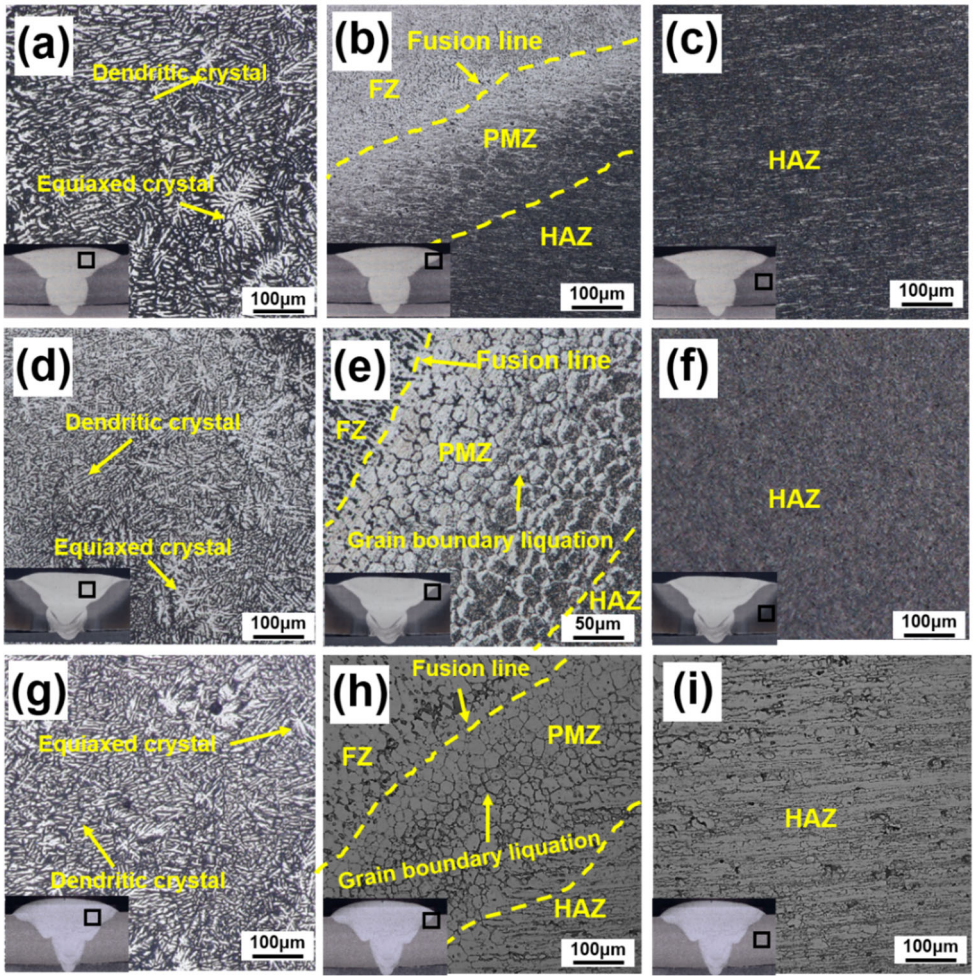


**Figure 4.** The microstructure of different aluminum alloy welded joints: 5083: (**a**) fusion zone (FZ), (**b**) partially melted zone (PMZ), (**c**) heat-affected zone (HAZ); 6005A: (**d**) FZ, (**e**) PMZ, (**f**) HAZ; 7N01: (**g**) FZ, (**h**) PMZ, (**i**) HAZ.

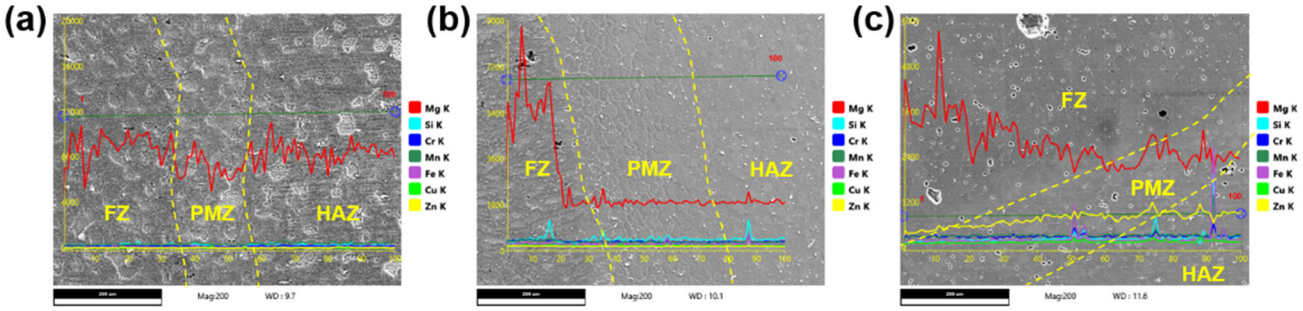


**Figure 5.** Energy-dispersive X-ray spectroscopy (EDS) scanning results of different aluminum alloy welded joints: (**a**) 5083; (**b**) 6005A; (**c**) 7N01.

The differential scanning calorimetry (DSC) curves of 5083, 6005A and 7N01 Al alloy was shown in Figure 6. Since the endothermic peaks in DSC curves implied a solid–liquid transition and the peak temperature of welding thermal cycles in the PMZ was between solidus line and liquidus line, the temperature ranges of endothermic peaks in DSC curves could associate with the extent of grain boundary liquation in the PMZ. The wider the temperature range was, the easier the grain boundary liquation generated in the PMZ. High liquation sensitivity indicated poor weldability, possibly leading to liquation cracking and decreasing joints strength under tensile stress. As demonstrated in Figure 6a, the temperature range of the coexistence of solid and liquid of 5083 Al alloy was between 610 °C and 640 °C, while the solid–liquid transition temperature of 6005A Al alloy ranged from 627 °C to 677 °C as depicted in Figure 6b. As for the DSC curves of 7N01 Al alloy shown in Figure 6c, two endothermic peaks could be found, with the ranges from 604 °C to 619 °C (peak A) and from 635 °C to 653 °C (peak B). Thus, the temperature range of solid-liquid coexistence of 6005A and 7N01 Al alloy was wider than that of 5083 Al alloy. The differences in the DSC curves revealed that 6005A and 7N01 Al alloys possessed severe liquation due to their wider solid–liquid transition temperature ranges. This result corresponded with the optical analysis depicted in Figure 3. Significant grain boundary liquation was obtained in the PMZ of 6005A and 7N01, while that of 5083 was slight. According to Huang C. et al. [26], the liquation cracking was closely related to the grain boundary liquation, and it can be inferred that 6005A and 7N01 aluminum alloy had higher liquation-cracking sensitivity than 5083 aluminum alloy, which was similar to the results reported in literature [27].

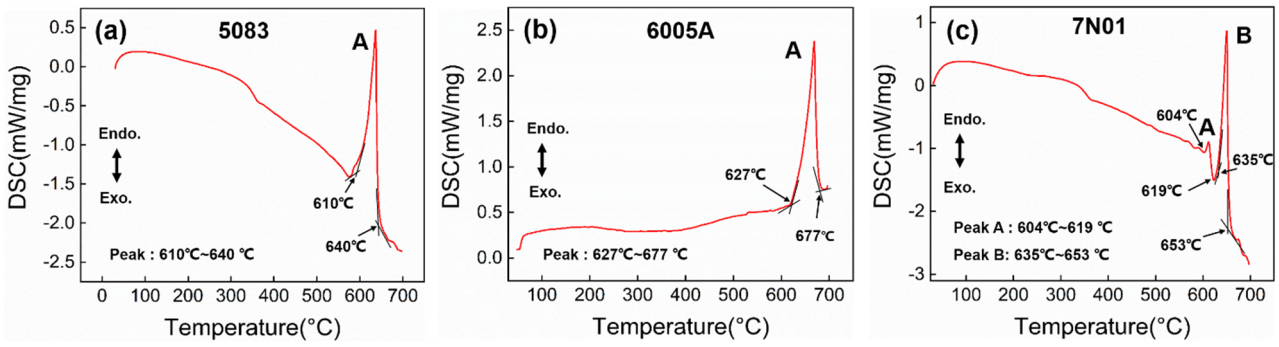


**Figure 6.** The differential scanning calorimetry (DSC) curves of different aluminum alloy joints: (**a**) 5083; (**b**) 6005A; (**c**) 7N01.

As mentioned above, recrystallization was obtained in the HAZ of 5083, 6005A and 7N01 Al alloys joints. To further study the distinction of the grain structure, EBSD analysis was conducted for the base metal and HAZ and the results are shown in Figure 7. Before welding, rolled-state grains with obvious crystallographic orientations were verified in the base metal as depicted in Figure 7a–c. After welding, the grain shape in the HAZ

changed due to the grain recrystallization induced by welding thermal cycle. In the HAZ of 5083 Al alloy, a coarse equiaxed grain was obtained as shown in Figure 7d. Besides, thinner equiaxed grains evolved from rolled-state grains were also observed in the HAZ of 6005A Al alloy as shown in Figure 7e. However, slight recrystallization was demonstrated in the HAZ of 7N01 Al alloy and the grain remained rolled shape as demonstrated in Figure 7f. Figure 8 displays the statistical data of grain size. Before welding, the grain size of the base metal in 5083, 6005A, and 7N01 Al alloys was 6.32, 4.74, and 5.32 μm, respectively. After welding, the grain size in the HAZ increased to 32.44, 18.39 and 22.31 μm, respectively. It can be seen that the degree of recrystallization of 5083 Al alloy was higher than that of 6005A and 7N01 Al alloy. This was because the recrystallization was mainly driven by thermal and strain effects. Severe lattice distortion caused by work-hardening in 5083 Al alloy increased additional driving force of grain recrystallization [28]. Although 5083, 6005A and 7N01 aluminum alloys joints experienced the same thermal cycles, the degree of recrystallization of 5083 Al alloy was higher than the other two. Owing to the diversity in original grain state and varied degree of recrystallization, different grain structures finally formed in the HAZ of the three aluminum alloys [29,30].

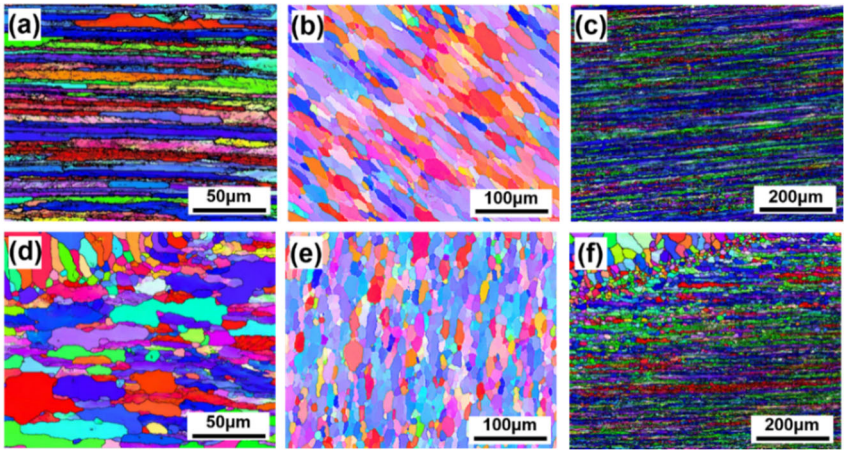


**Figure 7.** Electron backscatter diffraction detector (EBSD) images of aluminum alloy welding joints: 5083: (**a**) base metal (BM); (**d**) HAZ; 6005A: (**b**) BM; (**e**) HAZ; 7N01: (**c**) BM; (**f**) HAZ.

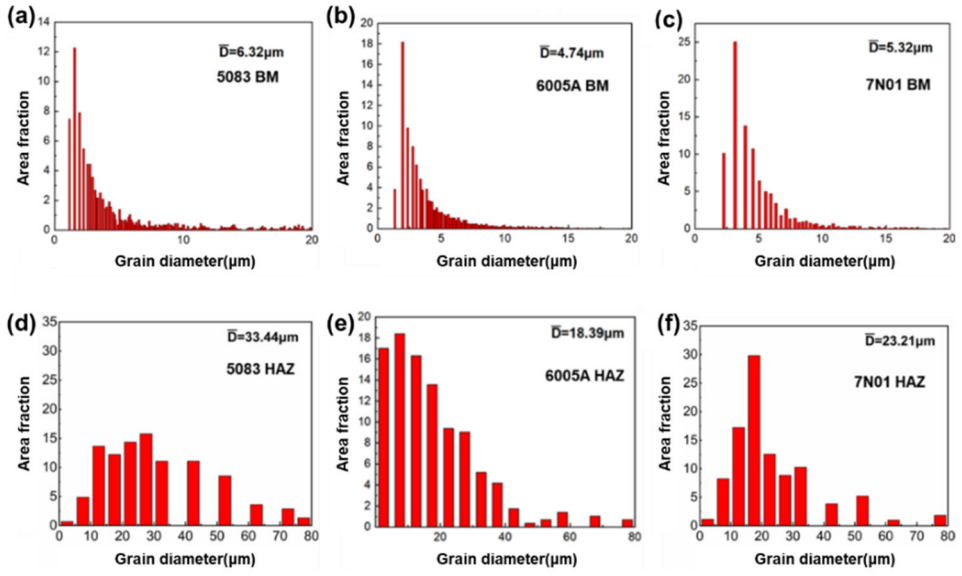


**Figure 8.** The grain size of different aluminum alloy welded joints: 5083: (**a**) BM; (**b**) HAZ; 6005A: (**c**) BM; (**d**) HAZ; 7N01: (**e**) BM; (**f**) HAZ.

Welding thermal cycles not only changed grain structure, but also affected the evolution of the second phases in the HAZ. Transmission electron microscopy (TEM) was used to observe the evolution of the second phases and the results are shown in Figures 9 and 10. According to element analysis in Figure 9, the tested region in HAZ consisted of α-Al, $Al_x$ (Mg, Mn), (Mg, Si), and (Mg, Zn) phases. Similar short rod-like shaped precipitates were observed in the HAZ of 5083 Al alloy before and after welding when comparing Figure 10a,d, implying that the second phase was less affected by thermal cycles. However, large changes were demonstrated in 6005A Al alloy joints. Before welding, a number of needle-shaped β″ ($Mg_xSi_y$) precipitates distributed in the matrix inducing strong precipitation strengthening effects (Figure 10b). After welding, the β″ precipitates significantly dissolved and turned into coarse round β phase as depicted in Figure 10e. As for the 7N01 Al alloy welded joints, a certain degree of reduction in the amount of η′ ($Mg_nZn_m$) precipitates was also observed in the HAZ compared with 7N01 Al alloy BM. The η′ phase ($Mg_nZn_m$) distributed in the HAZ before welding (Figure 10c). Part of η′ phase transformed into η phase ($MgZn_2$) under welding thermal effects (Figure 10f). The evolution of precipitates might influence the mechanical properties because precipitation-strengthening effects played an important role in enhancing the strength of 6xxx and 7xxx aluminum alloys.

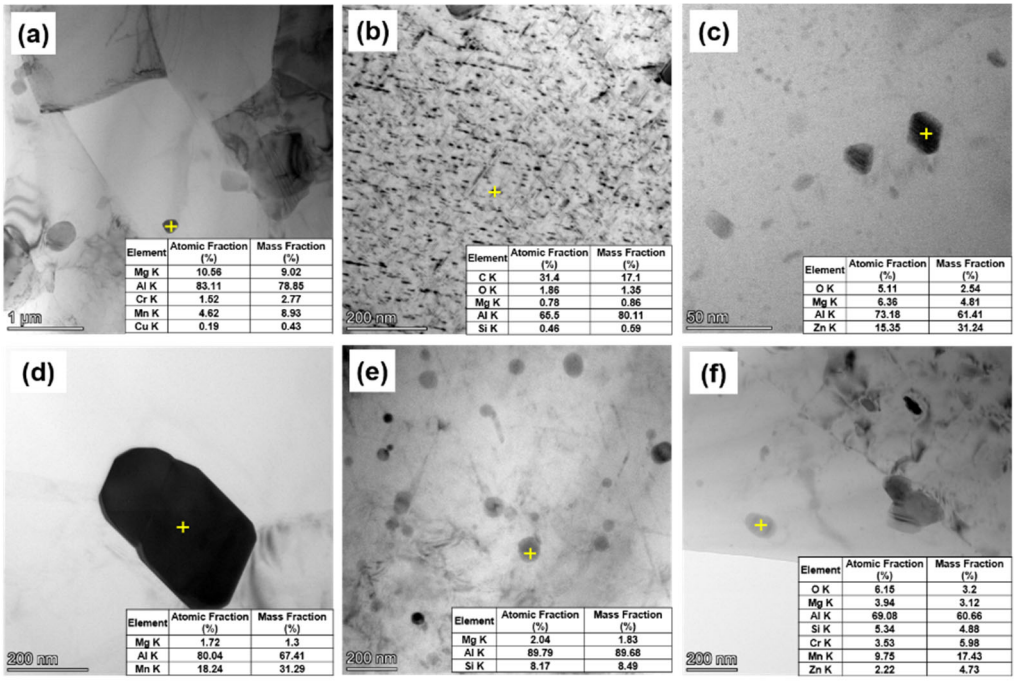


**Figure 9.** EDS results of different aluminum alloy welded joints: 5083: (**a**) BM; (**d**) HAZ; 6005A: (**b**) BM; (**e**) HAZ; 7N01: (**c**) BM, (**f**) HAZ.

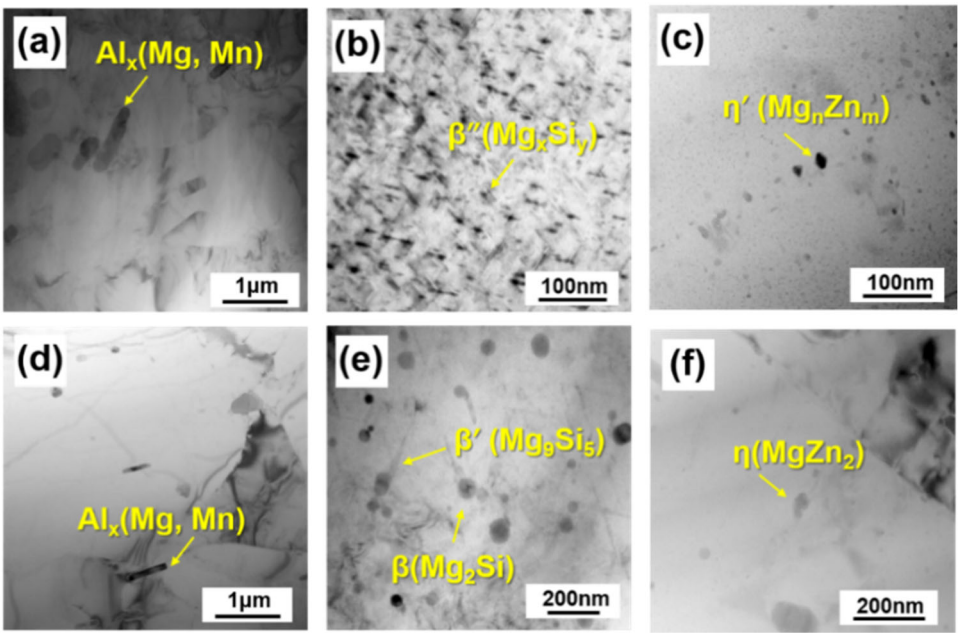


**Figure 10.** Bright-field transmission electron microscopy (TEM) micrograph of different aluminum alloy welded joints: 5083: (**a**) BM; (**d**) HAZ; 6005A: (**b**) BM; (**e**) HAZ; 7N01: (**c**) BM, (**f**) HAZ.

### *3.3. Mechanical Properties*

Figure 11 presents the microhardness profiles of 5083, 6005A and 7N01 Al alloy joints. The microhardness distribution of 5083 Al alloy joints remained consistent and slight fluctuations were observed at the center of welds as shown in Figure 11a. The average hardness value in welds was about 65 HV, which was lower than 84 HV of the base metal owing to lower strength of the filler metals. The microhardness distribution of 6005A joints was depicted in Figure 11b. The microhardness in the base metal was 98 HV while it reduced to 70 HV in the FZ. In the HAZ, the microhardness further decreased to 55 HV, implying the formation of a softening zone as marked in Figure 11b. The softening zone in the HAZ was mainly caused by the dissolution of β″ phases and grain recrystallization. Specifically, the β″ phase formed between 160 °C to 240 °C. When the temperature further increased during the welding process, the β″ coarsened and dissolved. Meanwhile, β′ formed between 240 °C and 380 °C. The β′ phase was unstable and transformed to β phase when HAZ rapidly cooled down. Then, the precipitation strengthening effect of β″ was much better than in β phases. In multi-layer GMAW, multiple thermal cycles further promote above processes. Therefore, the HAZ severely softened. Both the coarsened grains demonstrated by EBSD (Figure 8b,e) and the decrease in the number of precipitates verified by TEM (Figure 10b,e) deteriorated the microhardness of the HAZ. The microhardness profile of 7N01 Al alloy joints is displayed in Figure 11c. The minimum microhardness was obtained at the center of the welds and the value was 69 HV. The microhardness in the base metal was 120 HV. In the HAZ, a slight decrease was observed and the microhardness was about 98 HV. The difference in microhardness profiles indicated that the microstructure of HAZ in6005A Al alloy joints was significantly influenced by welding thermal cycles while that of 5083 and 7N01 Al alloy joints were hardly affected. The evolution of microstructure in the HAZ of 6005A Al alloy resulted in the microhardness loss.

The tensile test results are presented in Table 4 and strength-strain curves are shown in Figure 12. The tensile strength of 5083, 6005A and 7N01 Al alloy joints were 323, 206 and 361 MPa, respectively. The fracture positions of those joints are displayed in Figure 13. The 5083 Al alloy joints fractured at the fusion line. The 6005A Al alloy joints fractured at the HAZ while the 7N01 Al alloy joints failed at the FZ.

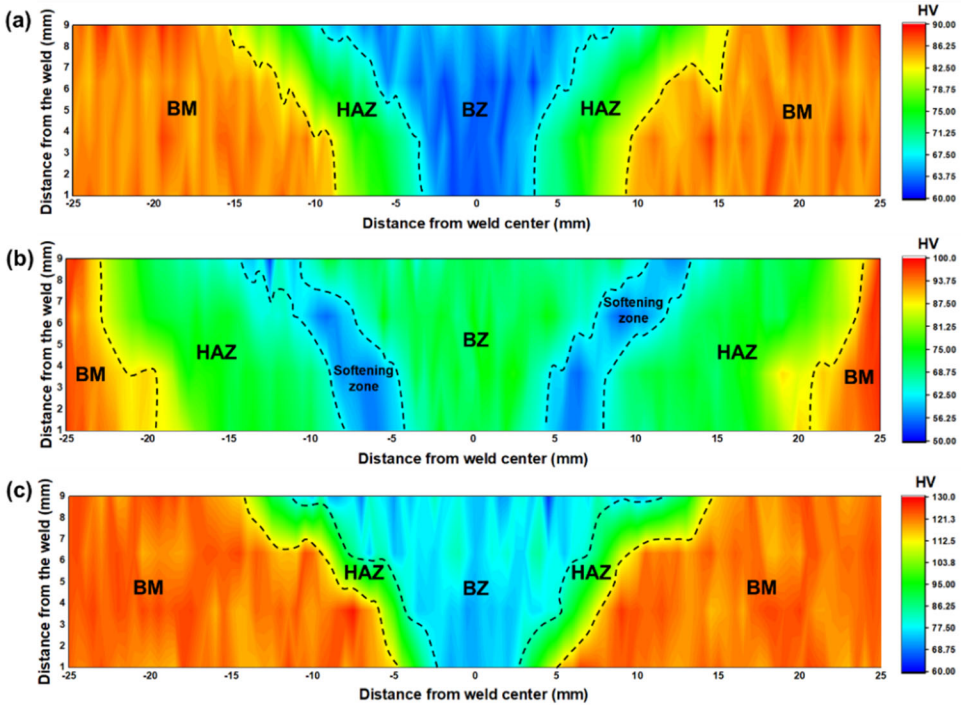


**Figure 11.** Microhardness profile of different aluminum alloy welded joints: (**a**) 5083; (**b**) 6005A; (**c**) 7N01.

The difference in strengthening mechanism and the evolution of microstructure for the three Al alloy resulted in different strength and fracture positions of the joints. For 6005A Al alloy, the strength loss caused by the dissolution of β″ precipitates was the main reason for the failure at the HAZ, because precipitation strengthening effects played an important role in enhancing the strength of 6005A Al alloy. The softer HAZ with low hardness severely deformed while the other region less deformed. The inconsistent deformation resulted in fast crack initiation and propagation in HAZ. Although the degrees of precipitate dissolution and grain boundary liquation were slight in 5083 Al alloy joints, the significant recrystallization in the region near the fusion line led to fracture at the fusion line, since lattice distortion caused by work-hardening mainly contributed to enhance the strength of 5083 Al alloy. At the same time, there were obvious Portevin-Le Chatelier (PLC) effects shown by the stress–strain curves of 5083 Al alloy joints including lots of serrations [31]. The PLC effect describes an unstable stress–strain response which was caused by dynamic strain aging (DSA) that arises from dynamic solute atom–dislocation interactions. Since 5083Al was a solid-solution hardening alloy, solute atoms might hinder dislocation movement under external tensile load. Consequently, the test sample was further hardened and the tensile curve rose. However, once tensile strain kept increasing in a short period and proceeded a certain value, dislocation could break the hindrance and abrupt softening was produced. The tensile curves then decreased. The above process was repeated promoting a serrated stress–strain curve [32–34]. As for 7N01 Al alloy joints, the base metal had the highest strength and the filler metal ER5356 for 7N01 Al alloy was low-strength matching. In addition, the grain structure and precipitates in 7N01 Al alloy joints were slightly affected. Therefore, the 7N01 Al alloy joints failed at the FZ with satisfying tensile properties.

**Table 4.** Detailed data of tensile test.

| Materials | | Tensile Strength (MPa) | | Elongation (%) | | Joint Efficiency (%) |
|---|---|---|---|---|---|---|
| 5083 | Sample 1 | 325.24 | 323.06 | 22.383 | 23.148 | 93.35 |
| | Sample 2 | 327.69 | | 20.691 | | |
| | Sample 3 | 316.27 | | 26.372 | | |
| 6005A | Sample 1 | 214.60 | 206.12 | 7.925 | 7.397 | 74.95 |
| | Sample 2 | 197.42 | | 6.717 | | |
| | Sample 3 | 206.34 | | 7.551 | | |
| 7N01 | Sample 1 | 362.16 | 361.33 | 9.800 | 10.378 | 96.52 |
| | Sample 2 | 365.34 | | 10.917 | | |
| | Sample 3 | 356.64 | | 10.417 | | |

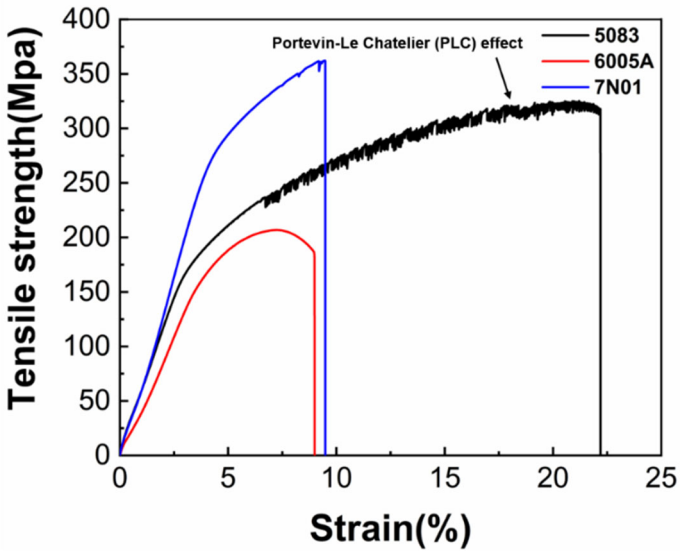


**Figure 12.** The displacement-strength curves of 5083, 6005A and 7N01 Al alloys welded joints.

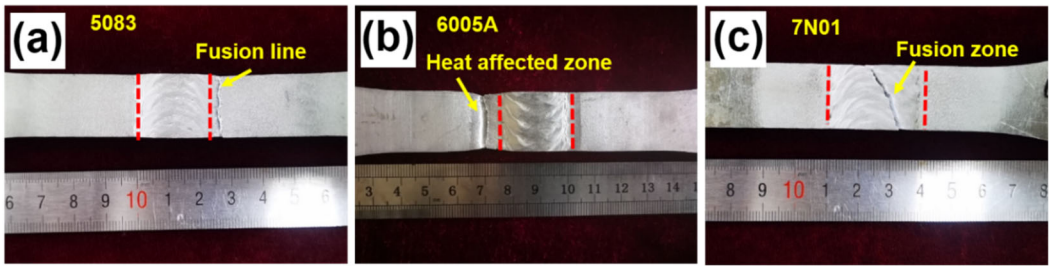


**Figure 13.** Fracture position of different aluminum alloy welded joints: (**a**) 5083; (**b**) 6005A; (**c**) 7N01.

Figure 14 shows the fractured surface of 5083, 6005A and 7N01 Al alloys joints from tensile testing. As shown in Figure 14a,d, the fracture surface of 5083 Al alloys joints was characterized by a number of dimples, a small amount short rod-like shaped precipitates and quasi-cleavage facets. This revealed an occurrence of ductile fractures. Figure 14b,e illustrate the fracture surface of 6005A. Larger and shallow dimples appeared on the fracture surface of 6005A Al alloy joints while quasi-cleavage could be found in a few places, which showed the ductile fracture was dominant [35]. Compared with the small and numerous dimples in 5083 aluminum alloy, the dimples in 6005A fractures showed poor mechanical properties. Figure 11c,f are characterized by the small, deep, dense dimples and almost without quasi-cleavage facets, which was evidence of the ductile type of fracture [36]. Compared with the fracture morphology of 5083 aluminum alloy, the dimples in the fracture of 7A01 aluminum alloy became smaller and denser, and no quasi-cleavage facets

and precipitates were found. The results implied the toughness of 6005A joints was lower than other joints.

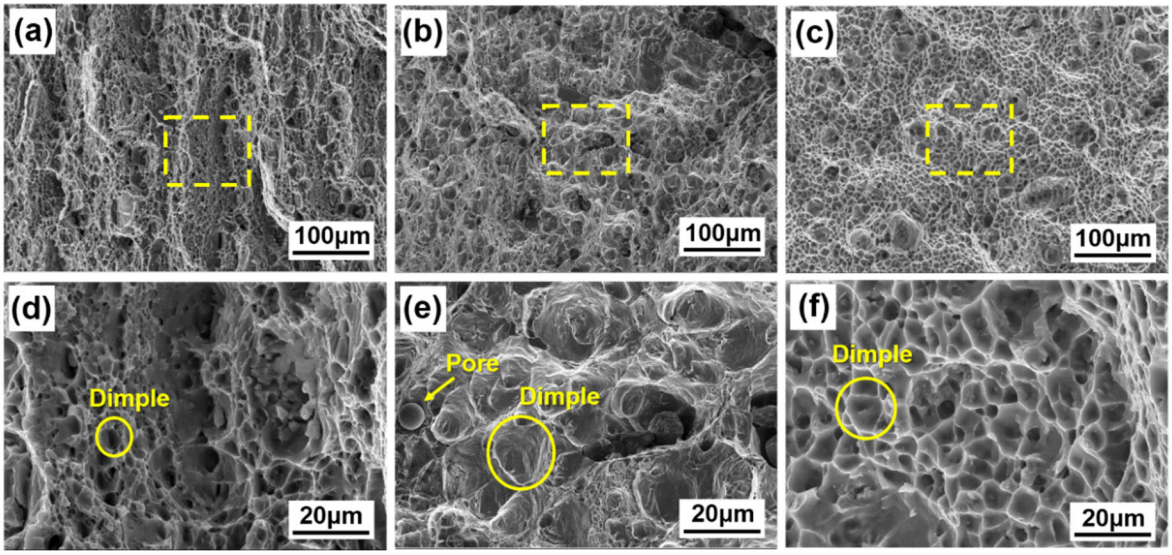


**Figure 14.** The fractured surface of different Al alloy joints: (**a**) and (**d**) for 5083; (**b**) and (**e**) for 6005A; (**c**) and (**f**) for 7N01.

### *3.4. Novelty and Application*

The 5083, 6005A, and 7N01 Al alloys are utilized in the train pillow beam of China Railway High-Speed trains as exhibited in Figure 15. A lock bottom structure was produced by aluminum profileI and plateII. In this study, a similar structure was built by butt joints with backing plates and used to undertake a comparative study, which, hopefully, provides significant guidance for choosing proper Al alloys in manufacturing the train pillow beam. The grain structure and precipitate evolution in the three kinds of Al joints was fully analyzed and critical mechanical properties were examined. The 6005A was precipitation-strengthened and most sensitive to welding thermal cycles, leading to the most severe softening and strength loss. The 5083 Al joints possessed better tensile properties and the strength of 7N01 joints was even higher. The PLC effects of the 5083Al joint reduced its processability. Although the joint strength is relatively low, 6005A has a low price and is still preferred in industries because it is easier to process, shape, and further surface treat, e.g., painting or oxidation. Service and design requirements should be carefully considered when choosing from those Al alloys.

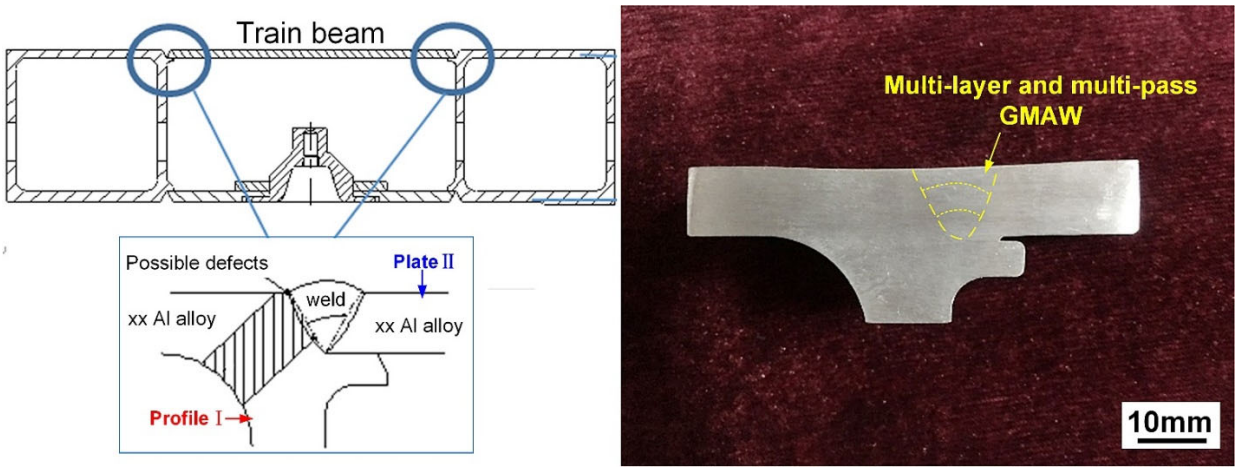


**Figure 15.** Aluminum alloys pillow beam in China Railway High-Speed trains.

## 4. Conclusions

(1) Successful joining of 5083, 6005A, 7N01 Al alloys was realized by a three-layer and three-pass GMAW process. The 6005A and 7N01 Al alloy joints possessed a higher degree of grain boundary liquation.
(2) Different extents of recrystallization were obtained in the three kinds of joint under the same thermal cycles. The recrystallization in 5083 Al alloy joints was the most severe while the grains in 7N01 Al alloy joints kept their original shapes with the lowest level of recrystallization.
(3) The precipitates in 5083 and 7N01 Al alloy joints were slightly affected by welding thermal cycles. However, the $\beta''$ precipitates in 6005A Al alloy joints significantly dissolved and coarsened, dramatically degrading the strength properties.
(4) The tensile strength of 5083, 6005A and 7N01 Al alloy joints were 323, 206 and 361 MPa, respectively. The 5083 and 7N01 Al alloy joints possessed high strength and could be used in force-bearing parts. Although the formability of 6005A were excellent, the severe strength loss of the softening zone must be considered in design.

**Author Contributions:** Data curation, B.X. and Y.L.; Investigation, L.W.; Methodology, G.M.; Project administration, X.H. and X.S.; Writing—original draft, L.W. and B.Y.; Writing—review and editing, C.T. All authors have read and agreed to the published version of the manuscript.

**Funding:** This research was funded by National Natural Science Foundation of China (52005132), the Natural Science Foundation of Shandong Province (ZR2019PEE038), the Heilongjiang Touyan Team, and CRRC Qingdao Sifang Co., Ltd. (Contact No. SF-JG-2020-159).

**Acknowledgments:** The authors are grateful to CRRC Qingdao Sifang Co., Ltd., for technical support with aluminum alloy welding experiments and the Heilongjiang Touyan Team for the funding support.

**Conflicts of Interest:** The authors declare no conflict of interest.

## References

1. Ke, W.; Bu, X.; Oliveira, J.; Xu, W.; Wang, Z.; Zeng, Z. Modeling and numerical study of keyhole-induced porosity formation in laser beam oscillating welding of 5A06 aluminum alloy. *Opt. Laser Technol.* **2021**, *133*, 106540. [CrossRef]
2. Pereira, D.; Oliveira, J.P.; Santos, T.; Miranda, R.; Lourenço, F.; Gumpinger, J.; Bellarosa, R. Aluminium to Carbon Fibre Reinforced Polymer tubes joints produced by magnetic pulse welding. *Compos. Struct.* **2019**, *230*, 111512. [CrossRef]
3. Torzewski, J.; Grzelak, K.; Wachowski, M.; Kosturek, R. Microstructure and Low Cycle Fatigue Properties of AA5083 H111 Friction Stir Welded Joint. *Materials* **2020**, *13*, 2381. [CrossRef]
4. Nakamura, T.; Obikawa, T.; Nishizaki, I.; Enomoto, M.; Fang, Z. Friction Stir Welding of Non-Heat-Treatable High-Strength Alloy 5083-O. *Metals* **2018**, *8*, 208. [CrossRef]
5. Tamasgavabari, R.; Ebrahimi, A.R.; Abbasi, S.M.; Yazdipour, A.R. The effect of harmonic vibration with a frequency below the resonant range on the mechanical properties of AA-5083-H321 aluminum alloy GMAW welded parts. *Mater. Sci. Eng. A* **2018**, *736*, 248–257. [CrossRef]
6. Liu, Y.; Wang, W.; Xie, J.; Sun, S.; Wang, L.; Qian, Y.; Meng, Y.; Wei, Y. Microstructure and mechanical properties of aluminum 5083 weldments by gas tungsten arc and gas metal arc welding. *Mater. Sci. Eng. A* **2012**, *549*, 7–13. [CrossRef]
7. Ma, M.; Lai, R.; Qin, J.; Wang, B.; Liu, H.; Yi, D. Effect of weld reinforcement on tensile and fatigue properties of 5083 aluminum metal inert gas (MIG) welded joint: Experiments and numerical simulations. *Int. J. Fatigue* **2021**, *144*, 106046. [CrossRef]
8. Corigliano, P.; Crupi, V.; Pei, X.; Dong, P. DIC-based structural strain approach for low-cycle fatigue assessment of AA 5083 welded joints. *Theor. Appl. Fract. Mech.* **2021**, *116*, 103090. [CrossRef]
9. Guan, Q.; Sun, J.; Wang, W.Y.; Gao, J.; Zou, C.; Wang, J.; Tang, B.; Kou, H.; Wang, H.; Hou, J.; et al. Pitting Corrosion of Natural Aged Al–Mg–Si Extrusion Profile. *Materials* **2019**, *12*, 1081. [CrossRef] [PubMed]
10. Osten, J.; Milkereit, B.; Schick, C.; Kessler, O. Dissolution and Precipitation Behaviour during Continuous Heating of Al–Mg–Si Alloys in a Wide Range of Heating Rates. *Materials* **2015**, *8*, 2830–2848. [CrossRef]
11. Zedan, Y.; Houria, M.I.; Vanderesse, N.; Atmani, F.; Mirakhorli, F.; Nadeau, F.; Demers, V.; Bocher, P. Fatigue properties of continuous wave and pulsed wave laser cold-wire welding of thick section AA6005-T6 aluminum alloys. *Int. J. Fatigue* **2021**, *147*, 106184. [CrossRef]
12. Bamberg, P.; Seewald, R.; Schiebahn, A.; Reisgen, U.; Precoma, N.; Epperlein, M. Improvement of the resistance spot welding of Al-Mg-Si alloys by using cladding technology: An optical and mechanical characterization study. *J. Adv. Join. Process.* **2022**, *5*, 100090. [CrossRef]

13. Dong, P.; Sun, D.; Li, H. Natural aging behaviour of friction stir welded 6005A-T6 aluminium alloy. *Mater. Sci. Eng. A* **2013**, *576*, 29–35. [CrossRef]
14. Liu, H.; Yang, S.; Xie, C.; Zhang, Q.; Cao, Y. Microstructure characterization and mechanism of fatigue crack initiation near pores for 6005A CMT welded joint. *Mater. Sci. Eng. A* **2017**, *707*, 22–29. [CrossRef]
15. Liu, H.; Yang, S.; Xie, C.; Zhang, Q.; Cao, Y. Mechanisms of fatigue crack initiation and propagation in 6005A CMT welded joint. *J. Alloy. Compd.* **2018**, *741*, 188–196. [CrossRef]
16. Kang, M.; Han, H.N.; Kim, C. Microstructure and Solidification Crack Susceptibility of Al 6014 Molten Alloy Subjected to a Spatially Oscillated Laser Beam. *Materials* **2018**, *11*, 648. [CrossRef]
17. Verma, R.P.; Pandey, K. Multi-response optimization of process parameters of GMA welding of dissimilar AA 6061-T6 and AA 5083-O aluminium alloy for optimal mechanical properties. *Mater. Today Proc.* **2021**, *46*, 10204–10210. [CrossRef]
18. Wang, H.; Zhang, J.; Wang, B.; Ma, M.; Yi, D. Influence of surface enhanced treatment on microstructure and fatigue performance of 6005A aluminum alloy welded joint. *J. Manuf. Process.* **2020**, *60*, 563–572. [CrossRef]
19. Li, Y.; Qin, W.; Yu, S.; La, J.; Fu, Y.; Li, J.; Yang, W.; Zhan, Y. Effect of Aging Treatment on the Corrosion Resistance Properties of 7N01 Extrusion Aluminum Alloy. *Materials* **2021**, *14*, 3615. [CrossRef]
20. Li, S.; Dong, H.; Shi, L.; Wang, X.; Liu, Z.; Shangguan, L.; Tian, Y. The Effects of Heat Straightening Temperature on the Microstructure and Properties of 7N01 Aluminum Alloy. *Materials* **2019**, *12*, 2949. [CrossRef]
21. Zheng, G.; Li, H.; Lei, C.; Fu, J.; Bian, T.; Yang, J. Natural aging behaviors and mechanisms of 7050 and 5A90 Al alloys: A comparative study. *Mater. Sci. Eng. A* **2018**, *718*, 157–164. [CrossRef]
22. Zhang, H.; Liu, H.; Song, J.; Guan, Q.; Ji, Z. Micro-characteristic and formation mechanism of layered band structure in non-weld-thinning friction stir welded 7N01 aluminum alloy. *J. Manuf. Process.* **2020**, *50*, 154–160. [CrossRef]
23. Zhang, Z.; He, C.; Li, Y.; Yu, L.; Zhao, S.; Zhao, X. Effects of ultrasonic assisted friction stir welding on flow behavior, microstructure and mechanical properties of 7N01-T4 aluminum alloy joints. *J. Mater. Sci. Technol.* **2020**, *43*, 1–13. [CrossRef]
24. Li, S.; Dong, H.; Wang, X.; Liu, Z.; Tan, Z.; Shangguan, L.; Lu, Q.; Zhong, S. Effect of repair welding on microstructure and mechanical properties of 7N01 aluminum alloy MIG welded joint. *J. Manuf. Process.* **2020**, *54*, 80–88. [CrossRef]
25. Lezaack, M.B.; Simar, A. Avoiding abnormal grain growth in thick 7XXX aluminium alloy friction stir welds during T6 post heat treatments. *Mater. Sci. Eng. A* **2021**, *807*, 140901. [CrossRef]
26. Huang, C.; Cao, G.; Kou, S. Liquation cracking in partial penetration aluminium welds: Assessing tendencies to liquate, crack and backfill. *Sci. Technol. Weld. Join.* **2004**, *9*, 149–157. [CrossRef]
27. Huang, C.; Kou, S. Liquation mechanisms in multicomponent aluminum alloys during welding. *Weld. J.* **2002**, *81*, 211s–212s.
28. She, X.-W.; Jiang, X.-Q.; Wang, P.-Q.; Tang, B.-B.; Chen, K.; Liu, Y.-J.; Cao, W.-N. Relationship between microstructure and mechanical properties of 5083 aluminum alloy thick plate. *Trans. Nonferrous Met. Soc. China* **2020**, *30*, 1780–1789. [CrossRef]
29. Oliveira, J.P.; Barbosa, D.; Fernandes, F.M.B.; Miranda, R.M. Tungsten inert gas (TIG) welding of Ni-rich NiTi plates: Functional behavior. *Smart Mater. Struct.* **2016**, *25*, 03LT01. [CrossRef]
30. Oliveira, J.; Shen, J.; Zeng, Z.; Park, J.M.; Choi, Y.T.; Schell, N.; Maawad, E.; Zhou, N.; Kim, H.S. Dissimilar laser welding of a CoCrFeMnNi high entropy alloy to 316 stainless steel. *Scr. Mater.* **2021**, *206*, 114219. [CrossRef]
31. Mäkinen, T.; Karppinen, P.; Ovaska, M.; Laurson, L.; Alava, M.J. Propagating bands of plastic deformation in a metal alloy as critical avalanches. *Sci. Adv.* **2020**, *6*, eabc7350. [CrossRef]
32. Gao, W.; Wang, D.; Seifi, M.; Lewandowski, J.J. Anisotropy of corrosion and environmental cracking in AA5083-H128 Al-Mg alloy. *Mater. Sci. Eng. A* **2018**, *730*, 367–379. [CrossRef]
33. Krishna, K.; Sekhar, K.C.; Tejas, R.; Krishna, N.N.; Sivaprasad, K.; Narayanasamy, R.; Venkateswarlu, K. Effect of cryorolling on the mechanical properties of AA5083 alloy and the Portevin–Le Chatelier phenomenon. *Mater. Des.* **2015**, *67*, 107–117. [CrossRef]
34. Aboulfadl, H.; Deges, J.; Choi, P.; Raabe, D. Dynamic strain aging studied at the atomic scale. *Acta Mater.* **2015**, *86*, 34–42. [CrossRef]
35. Blach, J.; Falat, L.; Ševc, P. Fracture characteristics of thermally exposed 9Cr–1Mo steel after tensile and impact testing at room temperature. *Eng. Fail. Anal.* **2009**, *16*, 1397–1403. [CrossRef]
36. Saini, N.; Pandey, C.; Mahapatra, M.M.; Narang, H.; Mulik, R.; Kumar, P. A comparative study of ductile-brittle transition behavior and fractography of P91 and P92 steel. *Eng. Fail. Anal.* **2017**, *81*, 245–253. [CrossRef]